Probing light mediators at ultralow threshold energies with coherent elastic neutrino-nucleus scattering

James B. Dent,[1,2] Bhaskar Dutta,[3] Shu Liao,[3] Jayden L. Newstead,[4] Louis E. Strigari,[3] and Joel W. Walker[2,5]

[1]*Department of Physics, University of Louisiana at Lafayette, Lafayette, Louisiana 70504, USA*
[2]*Kavli Institute for Theoretical Physics, University of California,
Santa Barbara, California 93106-4030, USA*
[3]*Mitchell Institute for Fundamental Physics and Astronomy, Department of Physics and Astronomy,
Texas A&M University, College Station, Texas 77845, USA*
[4]*Department of Physics, Arizona State University, Tempe, Arizona 85287, USA*
[5]*Department of Physics, Sam Houston State University, Huntsville, Texas 77341, USA*

Light neutral mediators, with mass $\lesssim 1$ GeV, are common features of extensions to the Standard Model. Current astrophysical and terrestrial experiments have constrained the model parameter space, and planned experiments around the world promise continued improvement in sensitivity. In this paper we study the prospects for probing light neutral mediators using terrestrial stopped pion and reactor sources in combination with ultralow threshold nuclear and electron recoil detectors. We show that the coherent neutrino-nucleus and neutrino-electron scattering channels provide complementary sensitivity to light mediators. With low-threshold detectors, we show that most stringent bounds on models arise from the nuclear scattering process, improving upon previous bounds from electron scattering of solar neutrinos by nearly an order of magnitude for mediator masses $\gtrsim 0.1$ GeV.

I. INTRODUCTION

Low mass particles from hidden sectors occur in many extensions of the Standard Model (SM). Examples include grand unified theories, models that explain baryogenesis, or dark sector models that include a portal which provides a connection to SM particles. Many experiments around the world are now being developed to study light mediators and hidden sectors (see for example the review [1]).

Experiments that are designed to detect coherent elastic neutrino-nucleus scattering (CEνNS) can provide a particularly important probe of light mediator models. Because the CEνNS process is well predicted in the SM [2], a measured deviation from it can provide a test of beyond Standard Model (BSM) physics. These models include nonstandard neutrino interactions (NSIs) with new weakly coupled particles, electromagnetic properties of neutrinos, and oscillations into sterile neutrinos [3–13]. CEνNS can also shed light onto astrophysical processes occurring in neutron stars and core-collapse supernovae [14–18]. Neutrino oscillation experiments are also sensitive to NSI [19–21], however, low-threshold CEνNS experiments will be more sensitive to models of NSI with light mediators.

Although experiments to measure CEνNS [22,23] have been long proposed, recent experimental progress has made detection of CEνNS a reality. The COHERENT experiment[1] used a stopped pion beam at the Spallation Neutrino Source (SNS) to detect CEνNS with CsI detectors, measuring a cross section consistent with the Standard Model prediction [24]. The coherent neutrino-nucleus interaction experiment (CONNIE) experiment is currently using low-threshold CCD detectors near a gigawatt (GW) reactor source with near-term prospects for measuring the CEνNS process [25], and the Taiwan experiment on neutrino (TEXONO) experiment[2] is developing detectors to measure CEνNS also using a GW reactor neutrino source [26]. These experiments will be sensitive to BSM physics such as NSI and the neutrino magnetic moment [26]. More recently, the Mitchell Institute Neutrino Experiment at a Reactor (MINER)[3] at Texas A&M University has been developed to measure CEνNS using a megawatt (MW) reactor neutrino source, with sensitivity to sterile neutrinos, NSI, and the neutrino magnetic moment [11,12,27].

In addition to these terrestrial efforts, CEνNS will also be an important aspect of direct dark matter (DM) searches. Direct detection experiments search for the interaction of DM with SM particles, typically via the nuclear recoil induced by elastic DM-SM scattering. As direct detection experiments continue to increase in sensitivity, the solar, atmospheric, and diffuse neutrino background from CEνNS will become a pressing issue. For canonical parameterizations of the DM-nucleus cross section, the presence of the CEνNS background will result in a situation where increasing the experimental exposure typically does not improve the

---

[1]https://sites.duke.edu/coherent/
[2]http://www.phys.sinica.edu.tw/texono/
[3]http://miner.physics.tamu.edu/

sensitivity to lower cross sections, an obstacle known as the neutrino floor [28,29]. However, for more general parameterizations of DM interactions, the neutrino floor can be mitigated in a large fraction of the parameter space [30,31].

Several papers have studied how CEνNS can be used to probe light mediators. References [32,33] use solar neutrinos at direct detection experiments, studying dark photon models and generic light mediator interactions of scalar, pseudoscalar, vector, and axial-vector types. Reference [8] analyzes the sensitivity of several CEνNS experiments to light dark matter interacting with the SM through a light vector mediator coupled to the electromagnetic current.

In this paper we study the prospects for identifying NSI with light neutral mediators using a combination of CEνNS and neutrino-electron scattering experiments. New mediator particles whose masses are small compared to the typical momentum exchanged in the scattering process can significantly alter the scattering rate, with pronounced effects at low recoil kinetic energies ($\lesssim$keV), and are therefore an intriguing experimental target. We focus specifically on projections for the MINER experiment and the first phase of the COHERENT project, using a simplified model approach to project constraints on hidden sector models which include a new light vector boson that couples neutrinos to the lepton and quark sectors of the SM. We show that an experiment with the sensitivity of MINER can produce world-leading constraints on a $U(1)_{B-L}$ extension of the SM. Interestingly, the most stringent bounds arise from the nuclear scattering process rather than electron scattering as in solar neutrino probes. This is because the largest solar fluxes correspond to relatively low-energy regions of the neutrino spectrum, with correspondingly soft nuclear recoils below current detection thresholds, whereas reactors combine moderate neutrino energies with a large local flux. The hope for experimentally leveraging advantages of the CEνNS process relies upon a continued push towards lower-threshold detector technologies, such as those actively being developed for direct DM searches. This program is especially central to the study of models with light mediators, given the described rate enhancement in the ultralow recoil energy regime.

The outline of this paper is as follows. Section II briefly reviews some details of CEνNS in the SM, and Sec. III summarizes a generic simplified model extension of the SM that includes NSI via light mediators. Section IV describes the application of very-low-threshold detector technology to reactor searches. Section V briefly lays out the process employed for limit setting, and Sec. VI presents our main numerical sensitivity projections, including results for a specific $U(1)_{B-L}$ BSM model at MINER. In Sec. VII, we summarize and conclude.

II. CEνNS IN THE STANDARD MODEL

Coherent elastic neutrino-nucleus scattering has garnered great attention as an important process for astrophysics, dark matter physics, and as a test of the Standard

Model itself in a new, low-energy regime. The scattering proceeds due to a neutrino of incident energy E_ν impinging on a nuclear target, to which is imparted a kinetic recoil energy E_R. Coherent scattering arises as a pure quantum effect for incident neutrinos with small enough energy such that they are unable to probe the interior nucleon structure of the nucleus. Specifically, for momentum transfers $|\vec{q}| \lesssim R^{-1}$, with R the typical nuclear size, coherent scattering will generate an enhancement in the cross section.

The differential cross section for a neutrino scattering off of a target of mass m (such as an electron or quark) is

$$\frac{d\sigma}{dE_R} = \frac{G_F^2 m}{2\pi} \left((g_v + g_a)^2 + (g_v - g_a)^2 \left(1 - \frac{E_R}{E_\nu} \right)^2 + (g_a^2 - g_v^2) \frac{mE_R}{E_\nu^2} \right), \quad (1)$$

where G_F is the Fermi constant. The vector and axial-vector couplings $(g_v, g_a) \equiv (g_L + g_R, g_L - g_R) = (T_3 - 2Q_{em} \sin^2 \theta_W, T_3)$ are those of the scattering target with respect to the neutral current amplitude $(T_3 - Q_{em}\sin^2\theta_W)$ for coupling to a Z-boson, where T_3 is the diagonal generator of $SU(2)_L$, Q_{em} is the electromagnetic charge, and θ_W is the weak mixing angle. Note that the neutrino's charge under the neutral current t-channel exchange has already been globally factored out in Eq. (1). In the case that the neutrino scatters off of an electron, there is an additional interference diagram for the charged-current t-channel exchange of a W-boson where the final (ν_e, e^-) states are associated with crossed vertices. An analogous charged current interference diagram likewise exists for antineutrino scattering off of an electron, although it manifests instead via the s-channel. The functional form of Eq. (1) is unchanged by these additions, which may be absorbed into a simple redefinition of the scattering charges. Intuitively, the W exchange is pure left, adding a unit shift to each of (g_v, g_a). However, if the scattering source should happen to be of the antineutrino variety, as is the case for a nuclear reactor, then the entire effective axial charge inherits a relative negative phase, subsequent to conditional application of the positive unit shift for matched flavor. Intuitively, under CP, the inversion $(L \Leftrightarrow R)$ flips the sign of g_a. These transformations are summarized in Table I. The vector couplings to protons and neutrons are respectively $g_v^p = 1/2 - 2\sin^2 \theta_W$ and $g_v^n = -1/2$. The value of θ_W has been measured at energies of $\sim$10 MeV in atomic parity violation experiments [34], at

TABLE I. Summary of the vector and axial charges for the four scattering scenarios.

Source\Target	Nucleus	Electron
ν	(g_v, g_a)	$(g_v + 1, g_a + 1)$
$\bar{\nu}$	$(g_v, -g_a)$	$(g_v + 1, -(g_a + 1))$

energies of ∼1–8 MeV from reactor experiments [35], and has also been calculated in the $\overline{\text{MS}}$ scheme at low energies [36]; here we adopt the value $\sin^2\theta_W = 0.2387$. Radiative corrections to the couplings are also included as given by [4]. Given these values, one finds that the vector coupling to protons is subdominant compared to that for the neutrons. There is an additional complication for nuclear scattering, insomuch as one must account for the embedding of quarks into nucleons, which are in turn bound in the nucleus. This is a situation familiar from dark matter physics, with embedding prescriptions given for example in [37–40]. The axial part of the neutral current couples to the spin, which is not entirely due to the valence quarks [41]. Here we define the axial coupling for the proton (neutron) as a sum over the spin content,

$$g_a^{p(n)} = \sum_q g_a^q \Delta_q^{p(n)} \qquad (2)$$

where the $\Delta_q^{p(n)}$ are defined as[4]

$$\langle p(n)|\bar{q}\gamma_\mu\gamma^5 q|p(n)\rangle = 2\Delta_q^{p(n)} s_\mu^{p(n)}. \qquad (3)$$

Under this definition we can relate the axial couplings to the nucleon form factor, $g_A^{p(n)} = G_A^{p(n)}(q^2 \to 0) \approx g_A/2$. The total axial coupling to nuclei is proportional to the expectation value of the nucleon spin content in the nucleus, $\langle S_p \rangle$ and $\langle S_n \rangle$. These expectation values vary from element to element, with the values of interest in this work for germanium and silicon given by [42]. The vector and axial couplings add coherently over the nucleus; thus, the total vector and axial charges of the nuclei are

$$Q_v = g_v^p Z + g_v^n N, \qquad (4)$$

$$Q_a = g_a^p \langle S_p \rangle + g_a^n \langle S_n \rangle. \qquad (5)$$

The Helm form factor can be used to account for the loss of coherence as momentum transfer increases. We do not include a spin form factor as they do not vary much over the region of interest [43]. Putting this together, we can then write the SM neutrino-nucleus differential cross section as

$$\frac{d\sigma}{dE_r}(E_r, E_\nu) = \frac{G_F^2 m_N}{\pi}\left[\left(1 - \frac{m_N E_r}{2E_\nu^2}\right)Q_v^2 F^2(E_r) \right.$$
$$\left. + \left(1 + \frac{m_N E_r}{2E_\nu^2}\right)Q_a^2 \frac{4(J_N+1)}{3J_N}\right]. \qquad (6)$$

Given the spin pairing of nucleons, the net nuclear spin is approximately given by the unpaired nucleon, and thus in the SM the dominant contribution to CEνNS will arise from

---

[4]We take values of the spin content of the nucleons from [41]: $\Delta_u^p = \Delta_d^n = 0.830$, $\Delta_d^p = \Delta_u^n = -0.386$, and $\Delta_s^p = \Delta_s^n = -0.021$.

the vector coupling. Since g_v^p is small, this yields a total cross section that scales at leading order as N^2. When considering scattering from reactor neutrinos, the inclusion of the form factor only reduces the rate by a few percent; thus, we will not consider the uncertainties arising from the choice of form factor. It should be noted that the form factor has a much larger effect on the higher energy sources of neutrinos. For the case of electron scattering, we take the free electron approximation, whereby you only scatter from electrons for which the recoil has enough energy to liberate. This gives rise to sharp features at the atomic energy levels.

III. CEνNS IN SIMPLIFIED MODEL EXTENSIONS OF THE STANDARD MODEL

We next examine modifications to the leading CEνNS event profile induced by the presence of new neutral current light mediators. For this analysis we will turn to a simplified model framework, which is a minimal extension of the SM that includes a new mediating particle, along with its couplings to neutrinos, electrons, and quarks. We follow a path similar to that of [33], where neutral current mediators are introduced that transform as a scalar (S), pseudoscalar (PS), vector (V), or axial vector (AV) under the Lorentz group. We consider a general set of dimension-4 interaction operators, specified by the following Lagrangians:

$$\mathcal{L}_S \supset \phi(g_{\nu,\phi}\bar{\nu}\nu + g_{\ell,\phi}\bar{\ell}\ell + g_{q,\phi}\bar{q}q) \qquad (7)$$

$$\mathcal{L}_{PS} \supset \phi(g_{\nu,\phi}\bar{\nu}\nu - i(g_{\ell,\tilde{\phi}}\bar{\ell}\gamma^5\ell + g_{q,\tilde{\phi}}\bar{q}\gamma^5 q)) \qquad (8)$$

$$\mathcal{L}_V \supset Z'_\mu(g_{\nu,Z'}\bar{\nu}_L\gamma^\mu\nu_L + g_{\ell,Z'}\bar{\ell}\gamma^\mu\ell + g_{q,Z'}\bar{q}\gamma^\mu q) \qquad (9)$$

$$\mathcal{L}_{AV} \supset Z'_\mu(g_{\nu,Z'}\bar{\nu}_L\gamma^\mu\nu_L - g_{\ell,\tilde{Z}'}\bar{\ell}\gamma^\mu\gamma^5\ell - g_{q,\tilde{Z}'}\bar{q}\gamma^\mu\gamma^5 q). \qquad (10)$$

Light mediators can be experimentally allowed, if their coupling is very weak. In place of a four-point Fermi interaction vertex, there is in this case a product of three-point couplings over a propagator explicitly dependent upon the momentum transfer $t = -2E_R m$. A light vector or axial-vector mediator may be simply accommodated in a manner similar to the prior inclusion of charged current interference, via redefinition of the effective charges in Eq. (1). Defining the axial phase α of a target species X by $(g_{X,v}, g_{X,a}) \equiv g_{X,Z'} \times (\cos\alpha, \sin\alpha)$, the prescription for holistic inclusion of these processes is given by

$$(g_v, g_a) \Rightarrow (g_v, g_a) + \frac{g_{\nu,v}g_{X,v}}{\sqrt{2}G_F(2E_R m_X + M_{Z'}^2)}$$
$$\times (\cos\alpha, \pm\sin\alpha), \qquad (11)$$

where $(-)$ signs apply for the case of antineutrino scattering. Note that the transformation in Eq. (11) will correctly reproduce the corresponding entries in Table IV of Ref. [33]

when applied to the base neutral current cross section of Eq. (1), while also automatically generating all suppressed terms of higher order in E_R/E_ν. (For a more thorough discussion of what can be gleaned qualitatively from the inclusion of a new mediating particle, see Appendix A.)

The possibility of a scalar or pseudoscalar mediator ϕ has several clear distinctions from that of a neutral vector mediator. Most essentially, a scalar coupling to two spinors mixes left and right chiralities, as would a mass term, whereas the vector mediator necessitates the insertion of a vector of gamma matrices between the spinors, which will not mix chirality. If it exists, the right-handed neutrino chirality has no standard model interactions. Indeed, the solar or reactor source will consist of solely left-handed neutrinos (or right-handed antineutrinos). However, the described experimental construction is insensitive to the nature of the exiting neutrino, and there is no direct prohibition against a sterile neutrino playing this role. More importantly, however, given that the SM has no process with identical initial and final states, there will be no SM interference terms generated (again, these are not necessarily vital to prospects for detection). Additionally, the scalar and pseudoscalar scenarios are prohibited from mixing, such that only the squares of individual couplings

are referenced in the differential cross section. This has the additional interesting consequence that neutrino and anti-neutrino scattering are equivalent, and insensitive to relative inversions of phase. Additionally, incompatibility of the Lorentz structure implies that it is impossible in this case to tidily summarize the new physics as a shift in the couplings of the neutral current SM vector boson exchange. The addition of a single particle with couplings $[g_{X,\phi}, g_{X,\tilde{\phi}}] \equiv g_{X,\phi} \times [\cos\alpha_\phi, \sin\alpha_\phi]$ to the field ϕ, adds a new term to Eq. (1),

$$\frac{d\sigma}{dE_R} \supset \frac{g_{\nu,\phi}^2 g_{X,\phi}^2 (E_R^2 m_X + 2E_R m_X^2 \cos\alpha_\phi)}{8\pi E_\nu^2 (2E_R m_X + M_\phi^2)^2}. \quad (12)$$

In Fig. 1 we have plotted example recoil spectra for $\bar{\nu}_e-$ nucleus and $\bar{\nu}_e - e^-$ scattering in germanium and silicon detectors. These spectra highlight several important points: (i) the motivation for low-threshold detectors is obvious from the rise in the spectrum at low recoil energies, (ii) the new interactions can produce deviations from the SM that could be within reach for near-term experiments, (iii) the interference between the pure SM interaction and the SM plus simplified model interactions may produce destructive
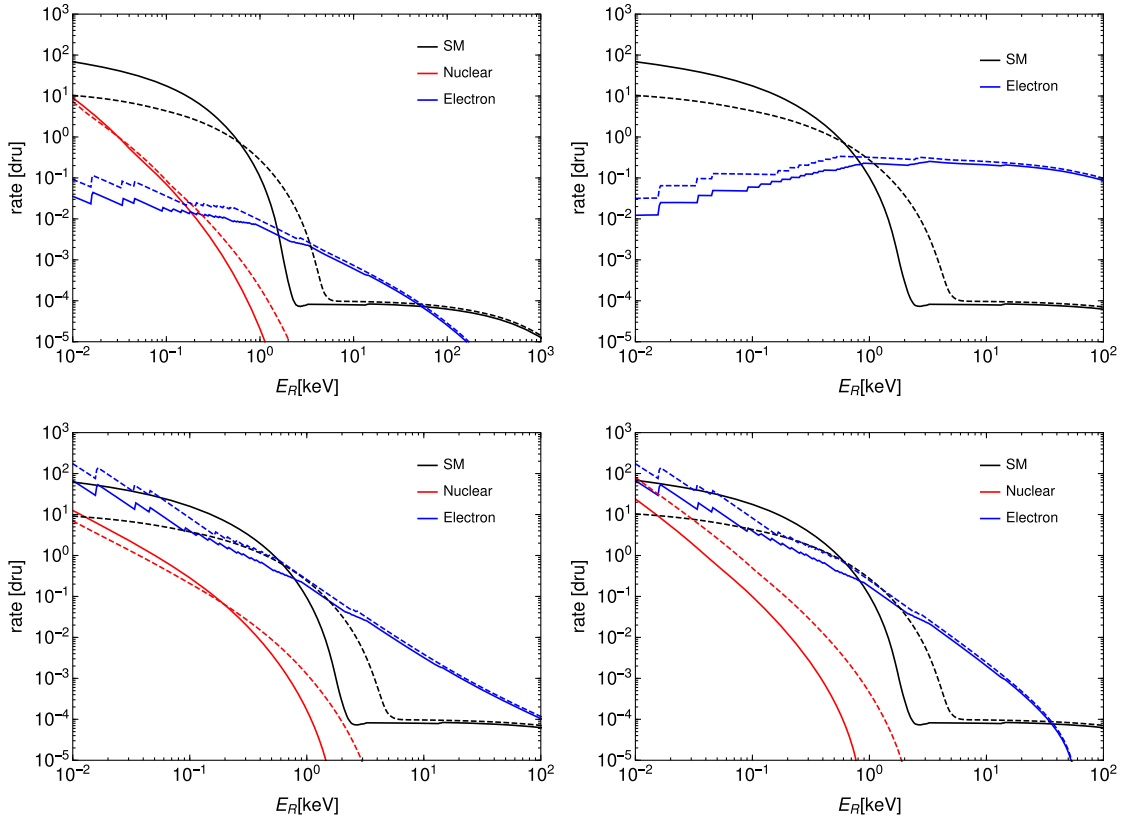

FIG. 1.   Sample recoil rates for the four BSM scenarios with the following mediator types: scalar (top left), pseudoscalar (top right), vector (bottom left), or axial vector (bottom right). The solid and dotted lines are for Ge and Si detectors respectively. The mediator mass is taken to be 1 keV and the coupling chosen such that the interaction is approximately the strength of the SM. The sharp features in the electron rates are due to atomic energy levels.

interference effects from V and AV exchange, and (iv) sharp features in the electron spectrum are due to passing threshold of the atomic energy levels. The shape of the spectra is dependent on the mediator mass, while the magnitude is dependent on both the mediator mass and coupling constants. For a 1 keV vector mediator to produce a rate similar to the SM at threshold, the couplings need to be of the order 10^{-6}.

IV. ULTRALOW THRESHOLD DETECTORS WITH REACTOR NEUTRINOS

In order to calculate the rate of recoil for nuclei we must specify the flux and energy distribution of incident neutrinos. Here we primarily consider reactor neutrinos, detected via CEνNS using ultralow threshold detectors. However, for comparison of sensitivity we will also consider solar neutrinos and stopped pion sources. These flux components are summarized in Table II.

To investigate the reach of reactor neutrino sources in probing NSI with light mediators, we consider the MINER experiment. As a brief review, the MINER program has been developed with the Nuclear Science Center at Texas A&M University (TAMU), which administrates a megawatt-class TRIGA-type pool reactor stocked with low enriched $(\sim 20\%)^{235}$U. Low-temperature solid-state germanium and silicon detectors, using technology similar to that currently developed for direct dark matter searches like SuperCDMS, will be installed at very near proximity ($\sim$1–3 m) to the reactor core. More specifics on the reactor, its properties, and the MINER program may be found in recent works which have highlighted its physics potential for TeV scale mass Z' models, sensitivity for neutrino magnetic moment searches, and sterile neutrino searches [11,12].

The antineutrino flux can be obtained via knowledge of the reactor's power (1.00 ± 0.02 MW in the present work) along with the normalized antineutrino fission spectrum, which has been measured at various sites (for a recent discussion of the current status of the spectrum see [45]).

TABLE II. Neutrino flux sources and their respective uncertainties in the flux normalizations. The SNS flux and uncertainty were taken from [24]. The solar components are derived from the high metallicity solar model as outlined in Ref. [44].

Component	ν flux (cm^{-2} s^{-1})
TAMU reactor (at 2 m)	$3.75(1 \pm 0.02) \times 10^{11}$
SNS (at 20 m)	
ν_μ (prompt)	$1.05(1 \pm 0.1) \times 10^7$
ν_e (delayed)	$1.05(1 \pm 0.1) \times 10^7$
$\bar{\nu}_\mu$ (delayed)	$1.05(1 \pm 0.1) \times 10^7$
Solar	
pp	$5.98(1 \pm 0.006) \times 10^{10}$
^{7}Be	$5.00(1 \pm 0.07) \times 10^9$
^{8}B	$5.58(1 \pm 0.14) \times 10^6$
pep	$1.44(1 \pm 0.012) \times 10^8$

The spectrum has not been directly measured below the 1.8 MeV inverse beta decay threshold. For these energies we adopt the theoretical distribution in Ref. [46]. Above 1.8 MeV we use the experimental results of Ref. [47].

We assume a detector exposure corresponding to germanium and silicon masses each of 10 kg, together with a five-year running time, as is realistic for the MINER experiment. As previously mentioned, an extremely important aspect of the detector technology is the existence of low thresholds for nuclear recoils (nr), due to the expected features in CEνNS that arise at recoil energies below the keV scale. We assume a 100 eVnr threshold for germanium and silicon. While no current technology exists that reaches such thresholds, experimental progress is underway which can reach these levels in the near future [48]. For example, CDMSlite recently achieved a threshold of 56 eVee (electron recoil) [49] and a few hundred eVnr (the exact conversion factor from eVee to eVnr depends on the parameterization for the ionization yield, which is only known to within a factor of a few). Given a sufficient number of events, the high resolution achieved by [48] will aid in resolving features in the differential rate. The proximity to the reactor, while ensuring a large neutrino flux, comes with a commensurately large neutron and gamma background. The goal for the MINER experiment is approximately 100 events per day per kg per keV, i.e., 100 dru, in the signal region. Modeling of the reactor, detector, and shielding show that this goal should be achievable [27], and thus we will use a flat background of 100 dru as a baseline. These detector specifications are summarized in Table III. In addition, we include a more optimistic future scenario (Ge II and Si II), to show the improvement that detector technology developments could yield.

The distribution of solar neutrinos presents either large flux at low energies, or low flux at large energies, as in Table II. The highest flux rates are from the pp process, integrating to approximately 6×10^{10} cm^{-2} s^{-1} and cutting off around 0.4 MeV, followed by the ^{7}Be and pep line sources at 0.9 and 1.4 MeV with corresponding fluxes 5×10^9 and 1×10^8 cm^{-2} s^{-1} (largely dominant over the N, O, F continuum), and the broad ^{8}B source that extends out to more than 15 MeV with an integrated flux of 6×10^6 cm^{-2} s^{-1}. In order to access the CEνNS process with near-term detector technology, it is necessary that the neutrino source have an energy in the few MeV range. For example, a nuclear recoil detector threshold around (20, 10) eV is required in (silicon, germanium) in order to register about half of the scattering events from neutrinos with a mean energy of 1.5 MeV [11]. The threshold scales as a square with E_ν, such that $E_\nu = 0.5$ MeV would require sensitivity at the level of about (5, 2.5) eV, approaching the theoretical limit for single electron ionization resolution [48]. Electron recoils require no such dramatic sensitivity, but they generally suffer with respect to rate and diffuse

TABLE III.   Detector specifications.

Name	Target	Exposure (kg day)	E_{th} (eV)	background (dru)
Ge	Germanium	10 000	100	100 ± 10
Ge II	Germanium	10 000	10	10 ± 1
Ge II(low BG)	Germanium	10 000	10	$(1 \pm 0.1) \times 10^{-4}$
Si	Silicon	10 000	100	100 ± 10
Si II	Silicon	10 000	20	10 ± 1
CsI	Caesium iodide	10 000	5000	$(1 \pm 0.05) \times 10^{-3}$

background contamination for the reasons described previously. For the spectral components where CEνNS could be presently visible, the flux is woefully low. By comparison, a nuclear reactor presents an (electron antineutrino) spectral composition distributed across the few MeV range that can exceed all of the solar flux by orders of magnitude, typically 10^{12-13} cm^{-2} s^{-1} [11,50,51]. This combination presents obvious advantages for the rate of signal events, although it likewise presents new challenges with respect to the management of radiologically intense backgrounds [27].

In addition to neutrinos from reactor and solar sources, stopped pion sources, such as at the SNS, produce neutrinos through the decay of muons at rest. These sources present the lowest fluxes, but at a much higher energy with a well-known flux. The higher energy allows the use of more conventional detectors with modest thresholds of a few keV, such as the CsI detectors employed in the first phase of the COHERENT experiment [52]. Values for the CsI detector efficiency and backgrounds were taken from [24]; here we will approximate the background as flat.

V. COMPUTATION OF CONFIDENCE INTERVALS AND LIMITS

Before competitive limits can be placed on new physics, the standard model CEνNS process must be discovered and measured. The MINER experiment can expect $\sim$10 dru from SM CEνNS, providing a signal-to-noise ratio of 1 : 10. From this we estimate that a 5σ signal will be observed with a few months of run time. To quantify how well the CEνNS

cross section can be measured we will use the profile likelihood test statistic,

$$t_\mu = -2 \log \frac{\mathcal{L}(\mu, \hat{\hat{\theta}})}{\mathcal{L}(\hat{\mu}, \hat{\theta})}, \tag{13}$$

where μ is the signal strength, $\frac{\sigma}{\sigma_{SM}}$, and θ represents the nuisance parameters. Hatted parameters, $\hat{\theta}$ and $\hat{\mu}$, denote the values which maximize the likelihood [note that the parameters $(\hat{\theta})$ which maximize the likelihood for a given μ may not be the same as the parameters $(\hat{\hat{\theta}})$ that maximize for $\hat{\mu}$]. We will use a binned likelihood function given by

$$\mathcal{L} = \prod_i \frac{\nu_i^{n_i} e^{-\nu_i}}{n_i!} \prod_j e^{-\frac{1}{2\sigma_j^2}(1-N_j)^2}. \tag{14}$$

Here ν_i and n_i are the expected (SM) and observed events in each bin, and the second product is a Gaussian likelihood summed over the nuisance parameters: the background and flux component normalizations N_j (one, three, and four components for the reactor, SNSm and solar cases respectively, where the values are given in Table II). The test statistic is then used to derive the expected 90% confidence intervals on the signal strength using the Asimov data set [53]. The Asimov data set is the set of simulated data which will cause the likelihood to be maximized at the expected points of all the parameters. Figure 2 shows the confidence intervals and discovery significance as a function of
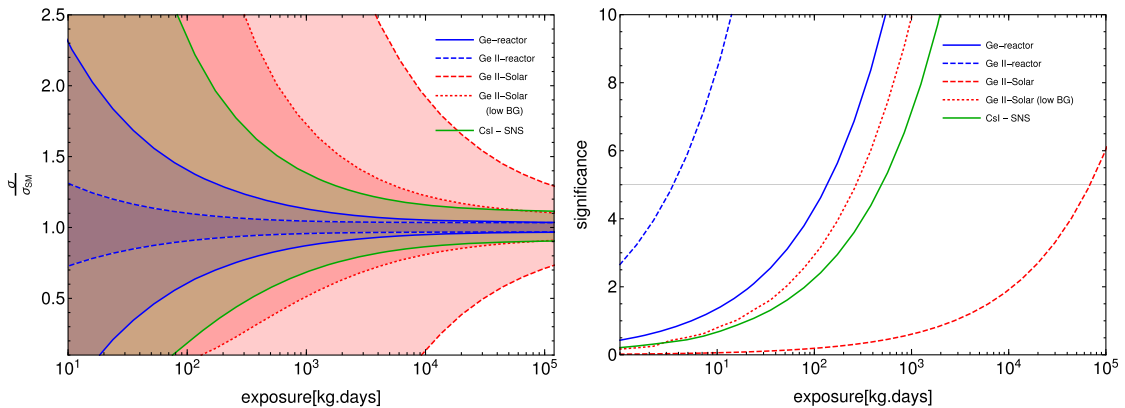

FIG. 2.   Left: 90% confidence intervals on the standard model CEνNS cross section from a selection of experiments. Right: Exposure required to reach a 5σ fluctuation from the background-only hypothesis.

exposure for several example experiments. The MINER experiment (situated at 2 m from the reactor) will be able to discover the SM process within 100 kg day and constrain the SM cross section to $\pm 10\%$ with 10^3 kg day of exposure, even with the conservative background and threshold assumptions. The solar and SNS neutrino experiments require roughly 100 times as much exposure to achieve the same discovery potential and measurement accuracy. This is due to the smaller fluxes and larger uncertainties in these experiments.

To investigate the experimental reach of the MINER experiment we calculate discovery limits for the detector configurations listed in Table III, based on the flux of the TAMU reactor at 2 m. The limits are also calculated for the same detectors with solar neutrinos as the source. For comparison with a current experiment we have also included the discovery limits for the first phase of the COHERENT experiment. The various neutrino sources cannot be distinguished by the detector, and thus the reactor and SNS cases should thus include the solar neutrinos as well, although the limits are displayed separately for illustration. Given that a dedicated solar experiment would likely be carried out deep underground (not in close proximity to a nuclear reactor), we have also included the calculation for a Ge II experiment in a background-free environment. The discovery limits are defined as the smallest signal that could produce a 3σ fluctuation 90% of the time. To find this limit we use a binned likelihood function, Eq. (14), with log-spaced bins. The likelihood is used to calculate the log-likelihood ratio and generate the test statistic q_0, from which we may estimate the expected median significance of an experiment via the Asimov data set [53],

$$q_0 = \begin{cases} -2\log\frac{\mathcal{L}(\mu=0,\hat{\hat{\theta}})}{\mathcal{L}(\hat{\mu},\hat{\theta})} & \sigma \geq \hat{\sigma} \\ 0 & \sigma < \hat{\sigma} \end{cases}. \tag{15}$$

VI. DISCOVERY LIMIT RESULTS

The discovery limits for each of the four BSM models are shown in Fig. 3. For nuclear scattering, the parameters f_n, b_n, and a_n shown in the plots are respectively the scalar, vector, and axial-vector nucleon couplings. In this analysis we opt to directly constrain the nucleon couplings, instead of assuming the coupling structure to individual quarks, thus remaining model independent. For details on how to calculate nuclear couplings from an underlying model see Refs. [33,54]. We assume no isospin violation, such that the corresponding coherency factors for the nucleus at large are simply $(Q'_s = f_n A)$, $(Q'_v = b_n A)$, and $(Q'_a = a_0\langle S\rangle)$. The Helm form factor is used to account for the loss of coherence for the S and V interactions. The limits from electron scattering directly constrain the product of the couplings, e.g., $g_{\nu,Z'}g_{e,Z'}$. A first glance through each of the

Fig. 3 plots will reveal an essentially similar "hockey stick" curve profile, the general shape of which can be understood in terms of the momentum transfer.

As the mediator mass is decreased, the cross section increases, and thus the experiments are sensitive to smaller values of the couplings. For heavier mediator masses, the coupling (or rather the product of mediator couplings to the neutrino and to the scattering target) sensitivity is diminished with a log-log slope of 2, due to effects of the new physics interaction and propagator in the large-mass (point-like interaction) regime, where one has a Fermi styled contribution $g_{\nu,Z'}g_{X,Z'}/M_{Z'}^2$. This ratio is constant along the $(\log g_{\nu,Z'}g_{X,Z'} = 2\log M_{Z'})$ line. Conversely, the mediator mass may be neglected when it becomes small compared to the momentum transfer. The relevant term here is $g_{\nu,Z'}g_{X,Z'}/2E_R m_X$, which corresponds to a flat coupling limit sensitivity. There is a transition regime that interpolates between these two asymptotes, wherein the coupling sensitivity bends smoothly. Looking again at the propagator, we can infer that this knee in the sensitivity should be centered around $M_{Z'} \simeq \sqrt{2E_R m_X}$. This knee occurs at a lower mediator mass for electron scattering since the momentum transfer is much smaller in that case. Limiting momentarily to the dominant vector interaction of Eq. (1), and factoring out couplings and constant terms, the functional dependence of the differential cross section may be very well approximated as a linearly declining function of E_R that cuts off at $E_R^{\max}$, as specified in Eq. (A2),

$$\frac{d\sigma}{dE_R} \underset{\sim}{\propto} 1 - \frac{E_R}{E_R^{\max}}. \tag{16}$$

It should be understood that the light vector mediator and scalar mediator interactions imply complications to this simplified structure, as in Eqs. (11) and (12) respectively, although certain universalities persist. For a detector sensitivity threshold $E_R^{\min}$, and considering a monochromatic neutrino source energy E_ν, the integrated area under this curve is $(E_R^{\max} - E_R^{\min})^2/2E_R^{\max}$, or simply $E_R^{\max}/2$ if the threshold $(E_R^{\min} \ll E_R^{\max})$ is much smaller than the cutoff. Likewise, the mean recoil is $\langle E_R\rangle = (2E_R^{\min} + E_R^{\max})/3$, and the standard deviation of the recoil is $\sigma_{E_R} = (E_R^{\max} - E_R^{\min})/3\sqrt{2}$. This suggests that the sensitivity knee for nuclear recoils should be centered around E_ν, or around the geometric mean $\sqrt{m_e E_\nu}$ for electron recoils. The propagated width in the mediator mass is $\sigma_{M_{Z'}} = \sqrt{m_X/2\langle E_R\rangle} \times \sigma_{E_R}$, which implies a fractional width $\sigma_{M_{Z'}}/M_{Z'} \simeq 1/2\sqrt{2}$ that is independent of m_X at leading order. However, for scattering that is widely spread across a continuum of source energies E_ν, the width will be additionally correspondingly broadened.

We may test the prior conclusions against the numerical results in Fig. 3. For germanium, the minimal neutrino energy that can create a recorded recoil (for head-on
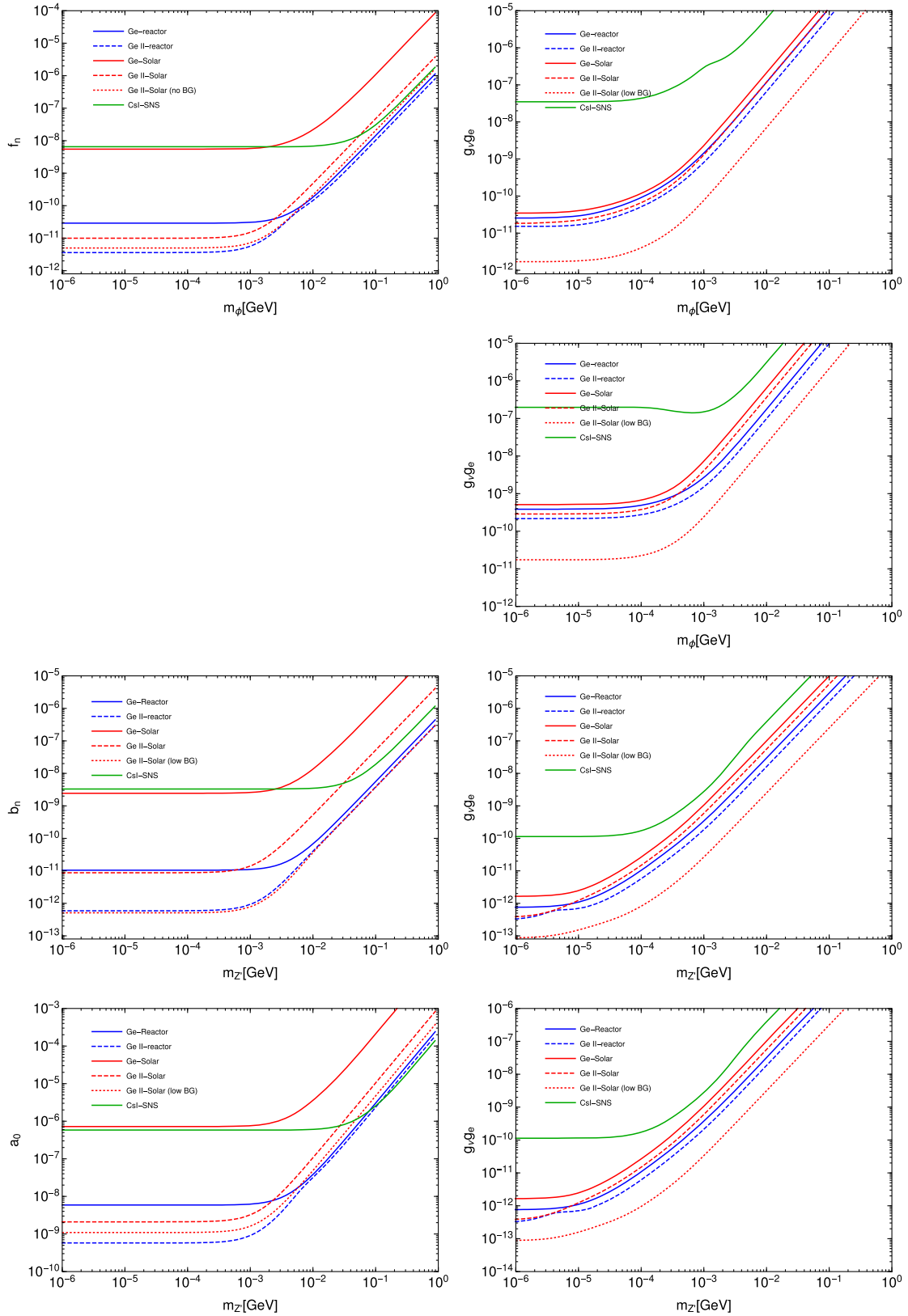
FIG. 3.   Discovery limits for neutrino scattering off germanium nuclei (left) and electrons (right), for the different BSM models: scalar, pseudoscalar, vector, and axial vector (from top to bottom).
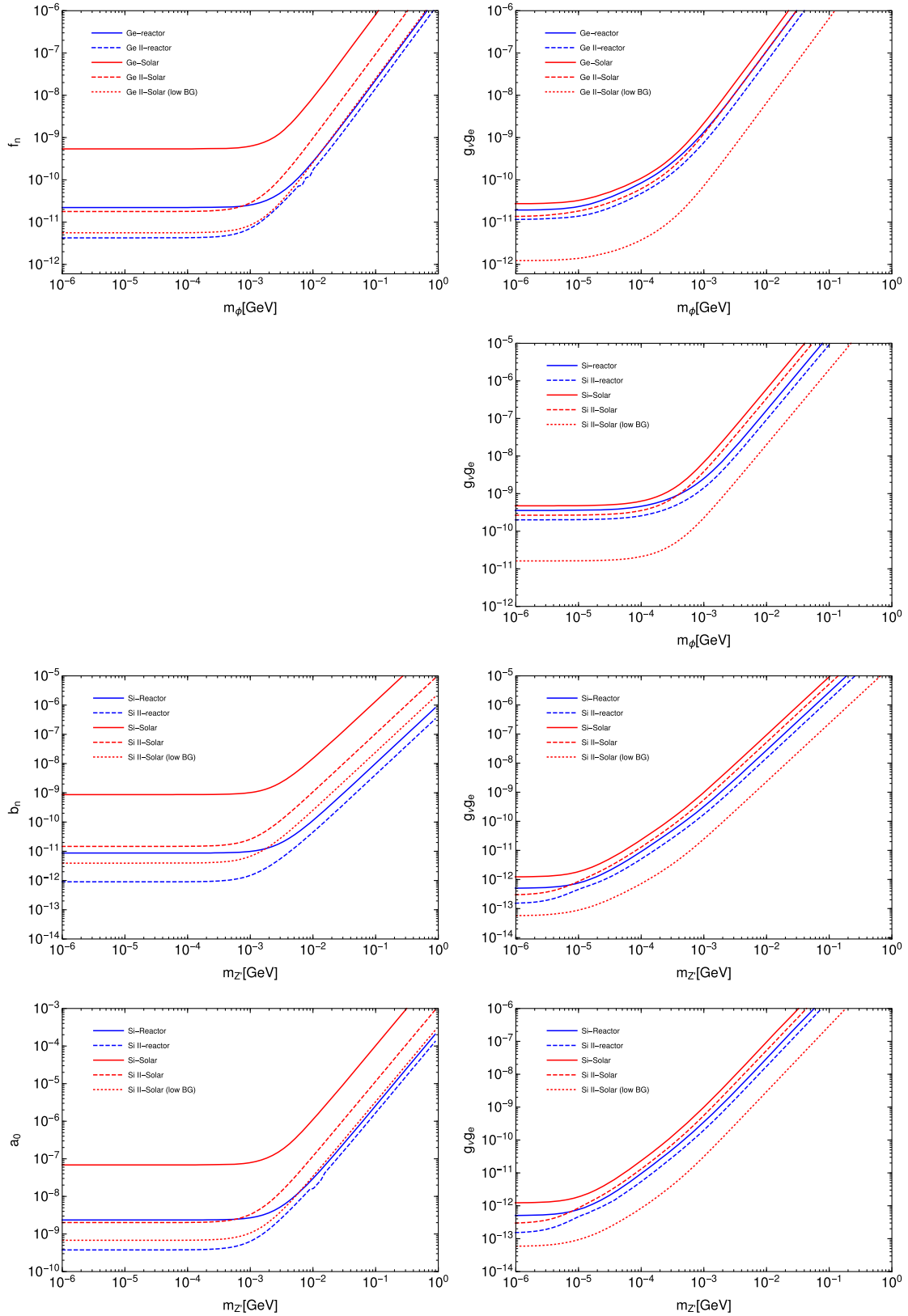
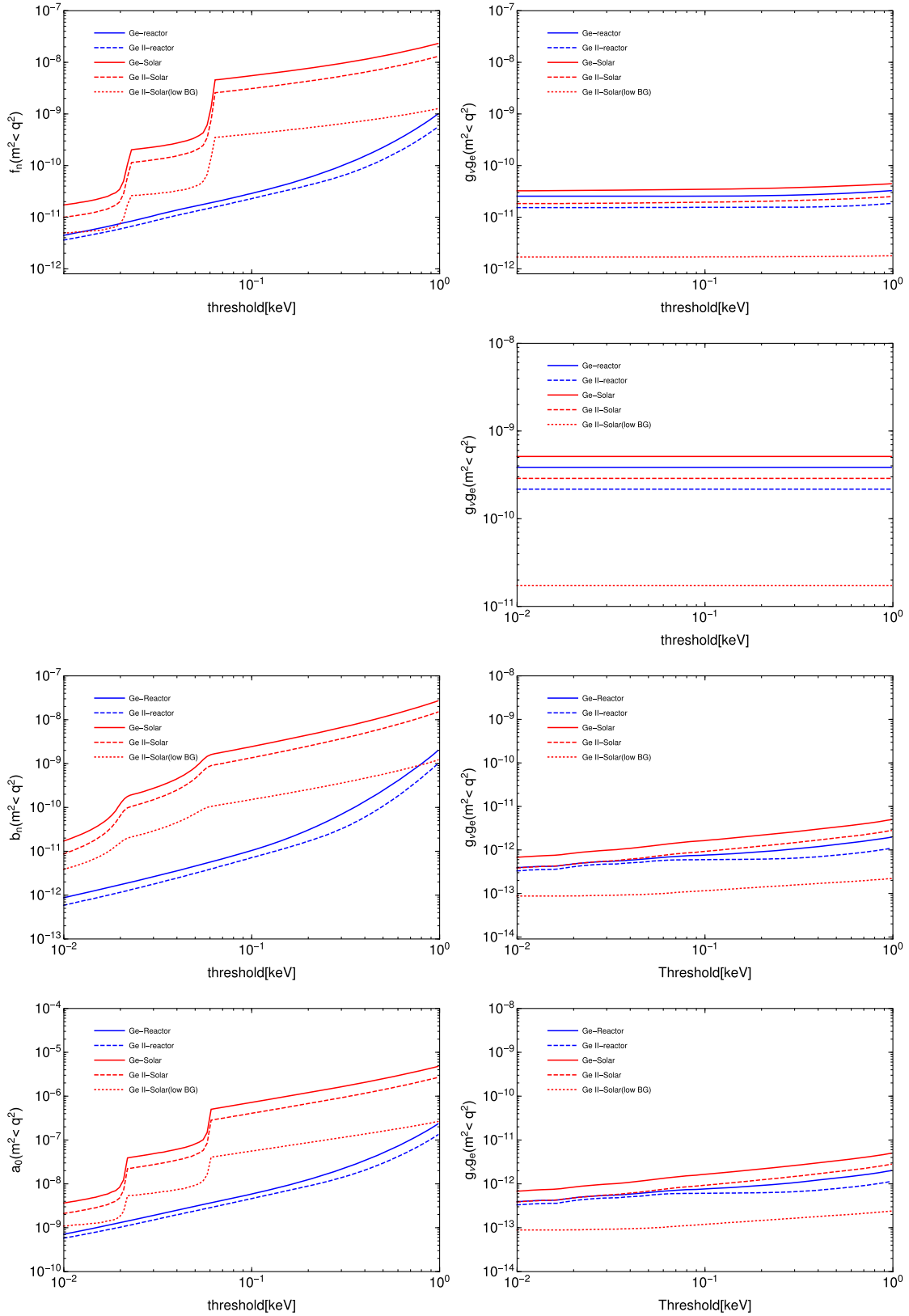FIG. 4.   The same as Fig. 3 but for silicon detectors.

FIG. 5.   Discovery limits vs threshold for neutrino scattering off germanium nuclei (left) and electrons (right), for the different BSM models: scalar, pseudoscalar, vector, and axial vector (from top to bottom).

collisions, which have the lowest cross section) is around 0.5 or 2 MeV, for threshold sensitivities $E_R^{\min}$ of 10 or 100 eV, respectively. Conversely, electron recoils can be sensitive to neutrinos as soft as a few keV. In the nuclear recoil column, we observe a rather sharp transition knee, centered at around mediator masses 1 to 4 MeV for the baseline and future threshold scenarios, which is stable across the different simplified models. As expected, each is a bit larger (about a factor of 2) than the kinematic turn-on. By eye the full width of the transition region is approximately 1 order of magnitude in mass. This suggests, consistently, that the continuum nature of the solar and reactor sources is relevant here. Looking at the electron scattering columns, we should expect a substantially wider transition region, which starts at much lower masses, because the lower reaches of the applicable neutrino energy spectra are not kinematically eclipsed. We should observe, furthermore, that there is a less appreciable leftward shift in the position of the knee for the second generation threshold sensitivity since most relevant electron scattering events are already integrated at very modest values of $E_R^{\min}$. Based simply on the very wide range of electron recoil energies E_R which are sampled, spanning from threshold near 100 eV up to more than 10 MeV, we can expect a transition region around the knee in $M_{Z'}$ that may cover more than 2 orders of magnitude, from approximately 10 keV up to a few MeV. We additionally observe more variation in the exact position and width of the knee between the four BSM models in the electron scattering case.

In Fig. 5, we plot the plateau sensitivity in the low-mediator-mass limit as a function of the experimental recoil threshold. As expected, going a lower threshold benefits the reach of the experiments, especially in the low-mediator-mass region. This effect is more pronounced for nuclear scattering since the electron scattering rate is flat with energy. The limiting factor of sensitivity to electron scattering is the background (which is also flat), when it is removed the sensitivity increases more than for nuclear scattering. The nuclear recoil plots clearly exhibit a stair-step behavior in sensitivity for the solar sources, as the ^{7}Be and pep line sources turn on at lower detection thresholds. Comparing individual experiments for a given BSM scenario, the larger flux of a reactor experiment allows for a greater reach when compared to an equivalent solar experiment. However, this gap is smaller when considering electron scattering, since the pp rate is able to contribute throughout the signal region, whereas for nuclei scattering the pp rate is below the detector threshold. Additionally, comparing with a solar experiment performed in a background-free environment, we find that the reactor experiments will still have a greater reach in most BSM scenarios explored. These conclusions are the same for the silicon experiments, the plots of which we have included in Fig. 4. In the proposed configuration the silicon detectors are underpowered compared to germanium, owing to the

smaller detector mass and fewer neutrons per nuclei. The utility of the silicon component of the experiment is in confirming a putative signal, not in adding statistical power to the overall sensitivity. Having two detector materials would also provide complementary information in the event of a discovery, for example, if there is isospin violation.

For further discussion and analysis of the discovery limits see Appendix B, where we develop an intuitive and predictive framework for assessing experimental sensitivity.

To compare the reach of a reactor experiment with a more general set of constraints we examine a $U(1)_{B-L}$ model with a light vector mediator of mass $m_{Z'}$ with coupling g_{B-L} described by the Lagrangian

$$\mathcal{L}_{B-L} \supset g_{B-L} Z'_\mu \left(\frac{1}{3} \bar{q}\gamma^\mu q - \bar{\nu}\gamma^\mu \nu - \bar{e}\gamma^\mu e \right). \quad (17)$$

This model has also been explored for CEνNS sourced by solar neutrinos with G2 and future direct detection experiments [32,33,55]. Figure 6 shows the reach in the g_{B-L} − $m_{Z'}$ space for the MINER scenario outlined above. The thick solid red curve gives the reach due to nuclear scattering, and the thick solid blue curve is the reach for electron scattering.

A few aspects of this plot are worth detailing. Interestingly we find that the nuclear scattering constraints are greater than those from electron scattering, which is a novel feature of the reactor experiment. Additionally, the reach for nuclear scattering from the reactor is well below
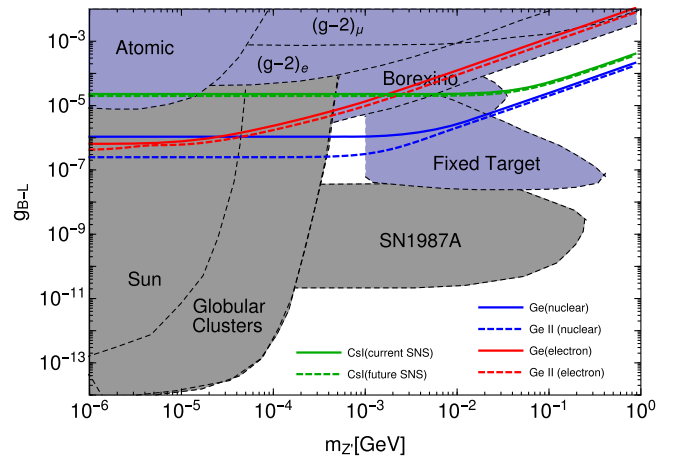

FIG. 6.　Predicted exclusion curves in the coupling-mediator mass parameter space in a $U(1)_{B-L}$ model for electron (red) and nuclear (blue) recoils observed by germanium detectors (phase I and II are solid and dashed respectively) with a total exposure of 10 000-days, thresholds situated 2 m from a $\bar{\nu}_e$ flux sourced by a 1 MW reactor. The green curves show the current (4466 kg day) and future (10 000 kg day) exclusion limits from the COHER-ENT experiment. The shaded regions are exclusion curves from other experiments and observations, a compilation from [32].

the reach for nuclear scattering from solar neutrinos. The blue and gray shaded regions are constraints from other experiments, whose details can be found for example in [32,33]. Thus, this demonstrates that a reactor experiment employing low-threshold detectors such as planned for MINER can provide world leading constraints in large regions of parameter space.

VII. CONCLUSION

Coherent elastic neutrino-nucleus scattering is a process with intriguing prospects for testing Standard Model physics and beyond. Though its measurement has been an experimental target for many years, only recently has technological innovations made an observation realistically imminent. With various collaborations such as COHERENT, CONNIE, TEXONO, and MINER currently taking data or planning to take data in the very near future, and with the possibility of using direct dark matter detection to test CEνNS through detection of the solar neutrino flux, the time is ripe to determine the extent to which these various experimental avenues can explore new physics.

In the present work we have examined the effect of new, light mediating particles on both the CEνNS process as well as electron scattering by neutrinos, by employing a simplified model approach including new scalar, pseudo-scalar, vector, and axial-vector mediators with sub-GeV masses. Such low-mass mediators can create a substantial enhancement in the rate of CEνNS and $\nu - e$ scattering at low recoil energies, further motivating the continued push towards low-threshold detector technology.

Within this simplified model framework we have determined the projected reach of experiments using low-threshold germanium and silicon detectors at a distance of ~1–3 m from the core of a MW-class nuclear reactor neutrino source (with the proposed MINER experimental configuration serving as a prototype), next-generation Ge and Si direct dark matter detection experiments, as well as the currently running CsI detector deployed by the COHERENT group at the SNS at Oakridge National Lab (the experimental parameters for these setups are given in Table III). Following other recent studies in this area, we have adopted a $U(1)_{\mathrm{B-L}}$ BSM framework, and found that low-threshold Ge detectors at close proximity to a nuclear reactor have superior prospects for probing this model, as demonstrated in Fig. 6. We have also provided scaling rules that bolster our numerical results, which also provide an intuitive guide to the discovery potential of the CEνNS and $\nu - e$ processes in the coupling and mass parameter space when new light mediators are considered.

Experimental groups are poised on the cusp of a first-ever measurement of the CEνNS process. Theoretical efforts such as those detailed in the present work, combined with continued progress on the experimental front, offer intriguing possibilities for near-term results within this exciting new region of particle physics.

APPENDIX A: A QUALITATIVE EXAMINATION OF NUCLEAR AND ELECTRON RECOILS FROM LIGHT MEDIATOR INTERACTIONS

In this appendix we will expound upon some of the interesting features arising in the scattering of nuclei and electrons from interactions mediated by light mediators. We will develop some intuition for interesting regimes of parameter space, discuss some interesting differences that arise when comparing electron to nuclear recoils, and revisit some pieces of conventional wisdom from neutrino scattering that are seen to no longer hold with the inclusion of light mediating particles.

We begin with an examination of the kinematics arising from the general formula of Eq. (11), reproduced here for convenience,

$$(g_v, g_a) \Rightarrow (g_v, g_a) + \frac{g_{\nu, Z'} g_{X, Z'}}{\sqrt{2} G_F (2 E_R m_X + M_{Z'}^2)}$$
$$\times (\cos \alpha, \pm \sin \alpha). \qquad (A1)$$

This equation gives the general means of including a new Z' vector or axial-vector mediating particle in addition to the Standard Model process.

For nuclear scattering, where $(E_\nu \ll m_N)$, we are guaranteed that $(E_R \ll E_\nu)$ will indeed apply. On the other hand, for electron scattering, with $(E_\nu \simeq m_e)$, it may similarly be that $E_R \simeq E_\nu$. However, investigation of the factor $2 E_R m_X + M_{Z'}^2$ from the Z' propagator suggests that the region of parameter space where terms of higher order in E_R / E_ν become relevant is typically disjoint from the region wherein the most substantial rate enhancement is derived from a light Z' mediator. Note first that the maximal kinetic recoil (for a head-on impact) impartable to a target of mass m_X is

$$E_R^{\max} = \frac{2 E_\nu^2}{m_X + 2 E_\nu}, \qquad (A2)$$

which reduces to the order of m_e for $(E_\nu \simeq m_e)$. In this case, $2 E_R m_e$ cannot be much greater than roughly $(m_e^2 \approx E_\nu^2)$, but it can be much, much smaller. This will be irrelevant if

$(M_{Z'} \gtrsim m_e)$, such that the mediator mass-square will always dominate, generating a flat response in E_R. However, if $(M_{Z'} \ll m_e)$, then the event rate is substantially enhanced as E_R decreases, scaling as E_R^{-2} (taking the square of the amplitude), until leveling off for recoils much below the knee $E_{R,e}^{\text{knee}} \equiv M_{Z'}^2/2m_e$. In particular, note that this cutoff for the rise in the light mediator enhancement occurs, given $(M_{Z'} \ll m_e \simeq E_\nu)$, in a regime where $E_R \ll E_\nu$. No such similar statement may be made about the neglect of terms of higher order in E_R/E_ν if $(M_{Z'} \gtrsim m_e)$. For the nuclear case, E_R^{max} reduces to $2E_\nu^2/m_N$ for $(E_\nu \ll m_N)$. As such, the relevant upper bound is $(2E_R m_N \leq 4E_\nu^2)$. Correspondingly, there will be no substantial variation of the light mediator enhancement with E_R unless $(M_{Z'} \ll E_\nu)$. If this is the case, then the event rate can again grow as E_R^{-2} until leveling off below an energy around $E_{R,N}^{\text{knee}} \equiv M_{Z'}^2/2m_N$. Note that even in the flat recoil response regime, which may onset more or less concurrently for both nuclear and electron scattering when $(M_{Z'}^2 \gtrsim 2E_R^{\text{max}} m_X \approx E_\nu^2)$, it remains possible, in principle, for the BSM rate to exceed the SM rate globally if $(M_{Z'}^2 \lesssim g_{\nu,Z'} g_{X,Z'}/G_F)$. All of the event features described here are purely kinematic, and are broadly independent of the specific couplings or spin of the hypothetical mediator.

There are two important bits of conventional wisdom developed in the approach to coherent nuclear scattering with heavy mediators that are now seen to be inapplicable, or at least not strictly applicable, to the case of scattering mediated by a light field. The first is that any NSI must have cross terms with the standard model in order to yield an appreciable rate. The usual intuition here (cf. Ref. [11]) is that NSI vertices, e.g., those representing a heavy gauge boson $(M_{Z'} \gg M_Z)$ with SM-comparable coupling strengths, will necessarily have amplitudes of substantially smaller magnitude than those of the SM, such that the leading new physics contribution in the square of summed amplitudes is from the interference term. A corollary of this statement is that new physics diagrams that cannot interfere with the SM, e.g., those representing flavor-changing neutral currents, will be practically invisible to experiments that are not sensitive to the final state on an event-by-event basis. For light mediators, it is quite conceivable that the failure of prior experiments to observe the corresponding signatures of new physics has been purely one of technology, namely the inability to probe very soft recoils of the target. Given a sufficient advance in technology to render the final state visible, it need not actually be weak, and a boost from interference with known SM processes is thus no longer a prerequisite to discovery. The second element of standard lore to be upended in the present context is that electron scattering is always subdominant to nuclear scattering in visibility at low recoil momenta. Support for this observation comes from two directions, the first being that only the nucleus is able to remain coherent for de Broglie wavelengths typical of nuclear energies, and thereby access the $\mathcal{O}(10^2)$ relative rate enhancement associated with summing over constituents in the amplitude prior to squaring. The second advantage (or sometimes disadvantage) of nuclear scattering is purely kinematic. The cutoff scale for recoil scattering E_R^{max} of a heavy nucleus may typically be a factor of 10^4 larger than the corresponding cutoff for electron recoil. Consequently, the nuclear recoil spectrum is highly concentrated inside a very narrow energy bandwidth, wherein its relative amplitude is correspondingly elevated. If the resultant recoils falls below threshold sensitivity of the detector, then they will be invisible. However, if the necessary threshold can be breached, a substantial gain in rate is attained. Whereas competing backgrounds to detection may have a very wide spectral composition, this isolation of a highly targeted integration domain is quite beneficial. Additionally, although event-by-event discrimination of nuclear from electron recoils is typically lost in solid-state detectors at very soft recoils (as the phonon vs ionization yield curves converge or the underlying phonon signal is traded for threshold sensitivity via Luke gain, cf. CDMSlite [49]) a reasonable amount of population discrimination may be recovered simply from this radical disparity of profiles.

In the regime $(M_{Z'}^2 \ll E_\nu^2)$, with typical MeV scale solar or reactor neutrino energies, both the electron and nuclear Z' scattering amplitudes will grow as $1/E_R$ with decreasing recoil energy, until flattening out at $(E_{R,X}^{\text{knee}} \simeq M_{Z'}^2/2m_X)$. In particular, the electron recoils will both onset $(E_{R,e}^{\text{max}}/E_{R,N}^{\text{max}} \simeq 10^4)$, and level off $(E_{R,e}^{\text{knee}}/E_{R,N}^{\text{knee}} \simeq 10^5)$, at much larger recoils for the same M'_Z. With identical couplings $g_{X,Z'}$, the single electron scattering to nuclear scattering (per particle constituent) amplitude ratio will grow linearly with increasing E_R, from parity below $E_{R,N}^{\text{knee}}$, up to a ceiling around 10^5 above $E_{R,e}^{\text{knee}}$. This advantage can, in principle, be more than sufficient to overcome the coherency advantage of the nucleus. However, the extended slow decline of the electron scattering rate across regions of the recoil parameter space well above several keV, which have historically been well instrumented and well probed, implies that the corresponding coupling must be very weak. Nevertheless, it may remain possible to skirt existing bounds while strongly enhancing the electron recoil at very low energies. For example, with $E_\nu = 2$ MeV, $M_{Z'} = 1$ keV, and $g_{\nu,Z'} g_{e,Z'} = 10^{-13}$, the new physics rate from electron scattering on a germanium target always exceeds the new rate from nuclear scattering, drops below the SM rate above 10 keV, and sharply exceeds the SM nuclear coherent scattering rate below about 15 eV, recovering the advantage of bandwidth compression conventionally held by the nuclear recoil. Moreover, this contribution may still be disentangled from the standard SM coherent nuclear scattering signal via identification of the characteristic E_R^2 power-law enhancement shape.

Interestingly, the electron recoil differential cross section can grow more rapidly (in a logarithmic sense) with increasing coupling than the nuclear recoil at low energies. The reason for this is that the new physics contribution will include both a cross term with the SM, and a square of the new physics amplitude, and the SM contribution is already large for the nuclear scattering case. When the new physics amplitude is smaller than the SM amplitude, the scaling with BSM couplings will be linear, but when the new physics amplitude is larger, the scaling with BSM couplings is quadratic.

APPENDIX B: SCALING RULES

In Sec. III, we intuitively characterized the shape and scale of contributions to the differential cross section for electron and nuclear scattering from the exchange of a new light mediator. In Secs. V and VI, we outlined the statistical machinery by which these profiles for new physics may be leveraged to set discovery limits, and plotted limit curves in the coupling vs mass plane for various assumptions of the mediator spin, coupling type, background control, and detector sensitivity. In the present appendix, we deconstruct this analysis approximately, but in closed form, in order to develop an intuitive predictive framework for assessing experimental sensitivity.

In particular, we consider the asymptotic coupling sensitivity in the massless mediator limit ($m_{Z'}^2 \ll 2E_R m_X$), and attempt to establish rules for the relative scaling of this limit with respect to variations such as the detector threshold $E_R^{\min}$, the neutrino source (solar or reactor) and energy E_ν, the target mass (either an electron or a nucleus), and the various BSM simplified models. In particular, we will attempt to develop a framework whereby one may approximately infer a family of related discovery limits from knowledge of any one member. In order to understand these relative sensitivities, it is essential to inspect the way that the discovery limit is calculated, in terms of the log-likelihood ratio q_0 defined in Eq. (15). After canceling the background contributions, and the nuisance parameter terms (neglecting subleading model dependencies in their optimization), we observe that any two models A and B will induce the same statistical deviation Δq_0 from the SM if $\log \mathcal{L}_A = \log \mathcal{L}_B$. Since all discovery limits will correspond to achieving a Δq_0 equal to certain Asimov number, we can use this condition to solve for the desired scaling factors.

For simplicity, we will reduce the binned likelihood in Eq. (14) to a single integration. Additionally, we notice that in the limit of large event counts, the Poisson distribution reduces to the Gaussian with expected number ν, observed number n, and standard deviation $\sigma = \sqrt{\nu}$,

$$-2 \log \mathcal{L} = \frac{(n-\nu)^2}{\nu}. \quad (B1)$$

Note that $(n - \nu)$ is the unified BSM event rate, including any potential mixing terms with the SM. We will have the same SM background rate ν for various models, so the criterion for comparison of limits reduces in this approximation simply to equality of (the absolute value of) the signal event deviation $|n - \nu|$, or equivalently to equality of the magnitude of the BSM cross section (allowing also for negative interference).

In order to extract simplified relationships on the new physics couplings Q', we need to isolate the leading terms, focusing now specifically on the nuclear scattering example. Given reasonable event rates and reliable background characterization, experiments will be sensitive to small deviations from the SM rate. The largest SM contributions are from the vector interaction, and this will enhance the cross term for BSM vector mediators. We define the coherent SM vector coupling to the nucleus as $Q_v \equiv -2 \times [Z g_v^p + (A - Z) g_v^n]$, consistent with Ref. [33]. Correspondingly, we may neglect the square of the new physics term in this case. By contrast, for axial-vector interactions, the mixing term with Q_v is of order $\mathcal{O}(E_R)$, and the mixing term proportional to Q_a is small because $Q_a \ll Q_v$. Thus, we may neglect mixing in this case, and take the square of the new physics amplitude to be leading. For the scalar interactions, no cross term with the SM exists. The associated cross sections are calculable,

$$n - \nu \underset{\sim}{\propto} \int_{E_R^{\min}} dE_R \int_{(E_R + \sqrt{E_R^2 + 2E_R m_N})/2} dE_\nu f(E_\nu)$$

$$\times \begin{cases} \frac{f_n^2 A^2}{16\pi E_\nu^2 E_R} & \text{scalar} \\[2ex] -\frac{b_n A G_F Q_v}{2\sqrt{2}\pi E_R}\left(1 - \frac{E_R}{E_R^{\max}}\right) & \text{vector} \\[2ex] \frac{a_0^2 \langle S \rangle^2}{8\pi m_N E_R^2}\left(1 + \frac{E_R}{E_R^{\max}}\right) & \text{axial vector,} \end{cases} \quad (B2)$$

where $f(E_\nu)$ is the antineutrino flux. For a monochromatic beam, we may integrate in closed form, retaining leading terms,

$$|n - \nu| \underset{\sim}{\propto} \begin{cases} f_n^2 \times c_s \equiv \frac{A^2}{16\pi E_\nu^2} \ln\left(\frac{E_R^{\max}}{E_R^{\min}}\right) & \text{scalar} \\[2ex] b_n \times c_v \equiv \frac{A G_F Q_v}{2\sqrt{2}\pi}\left[\ln\left(\frac{E_R^{\max}}{E_R^{\min}}\right) - 1\right] & \text{vector} \\[2ex] a_0^2 \times c_a \equiv \frac{\langle S \rangle^2}{8\pi m_N E_R^{\min}} & \text{axial vector} \end{cases} \quad .$$
$$(B3)$$

For a germanium target, we can take approximately $(A \to 73)$, $(m_N \to 68 \text{ GeV})$, $(Q_v \to 38)$, and $(\langle S \rangle \to 0.5)$, for ^{73}Ge with isotopic fraction $(\text{IF}_{73} = 0.08)$. Also, we have $G_F = 1.17 \times 10^{-5} \text{ GeV}^{-2}$. We will use $E_R^{\min} = 100 \text{ eV}$, corresponding to the first-generation experiment, and select a representative neutrino energy that is large enough to regularly trigger recoils above the threshold, say $E_\nu = 4 \text{ MeV}$, which implies $E_R^{\max} \simeq 470 \text{ eV}$. We may then estimate the relative limits $(b_n / f_n^2 \simeq c_s / c_v \to 5 \times 10^9)$,

and ($b_n/a_0^2 \simeq c_a \times IF_{73}/c_v \to 6 \times 10^4$), holding the event rate constant. Taking the calculated reactor flux limit ($b_n = 10^{-12}$) for the vector coupling, we can predict ($f_n \simeq 1 \times 10^{-11}$) and ($a_0 \simeq 4 \times 10^{-9}$) for the corresponding scalar and axial vector limits, which agree very closely with the detailed calculations illustrated in Fig. 3. Holding each of the Eq. (B3) integrated rates constant, we can extract slopes for variation of the coupling limits with respect to changes in the threshold $E_R^{\min}$,

$$
\begin{cases}
\frac{d \log f_n}{d \log E_R^{\min}} \simeq \frac{1}{2 \ln (E_R^{\max}/E_R^{\min})} & \text{scalar} \\[2mm]
\frac{d \log b_n}{d \log E_R^{\min}} \simeq \frac{1}{\ln (E_R^{\max}/E_R^{\min})-1} & \text{vector} \\[2mm]
\frac{d \log a_0}{d \log E_R^{\min}} \simeq \frac{1}{2} & \text{axial vector.}
\end{cases} \tag{B4}
$$

A typical value of $\ln (E_R^{\max}/E_R^{\min})$ is around 2. This suggests that each of the plots in the left-hand column of Fig. 5 should have a log-slope of order approximately 1, steepest for the vector case and trending steeper as one approaches the kinematic cutoff, which is broadly consistent with what is observed in the detailed calculation. The electron scattering plots are by contrast flat with respect to variation of the threshold. This is not because the rate does not increase at low recoils, but rather because the event rate in this region is typically dominated by nuclear recoils. In order to carry out a corresponding single-bin treatment of electron scattering, one would need to select an integration region which begins at a fixed scale around $E_R^{\min} \simeq 2$ keV, where the CEνNS differential cross section tapers off and is eclipsed by the electron rate, as in Fig. 1. A possible exception to this conventional scenario may arise for a sufficiently light mediator, if the electron rate is able to climb steadily in the keV region, to finally compete with the nuclear rate in the exceptionally soft recoil region, as described toward the end of Sec. III.

Next, we will briefly consider the relative strengths of limits achievable with solar and reactor sources in the case of nuclear scattering. Again, the strategy will be to hold the ratio $(n - \nu)^2/\nu$ constant. We observe that both the BSM signal and SM background will scale linearly with the integrated flux Φ, such that the ratio to be held constant is likewise linear in Φ. A first-generation experiment will be sensitive primarily to the ^{8}B continuum, whose net flux is diminished by a factor of $\mathcal{O}(10^5)$ relative to that of the reactor site under consideration at the bare minimal baseline. Additionally, however, there is sensitivity to the energy of the source, with the event rate scaling as E_ν^2. The mean energy of this solar source is a factor of a few larger than that of a terrestrial reactor, which offsets the rate advantage by approximately 1 order of magnitude, to $\mathcal{O}(10^4)$, in the square. The critical ratio $(n - \nu)^2/\nu$ is finally proportional to $\Phi \times (f_n^4, b_n^2, a_0^4)$ in the scalar, vector, and axial-vector models, after squaring the leading signal contributions from Eq. (B3). This suggests that the solar limits should be weaker by about a factor of 100 in the vector case, or about 10 in the scalar and axial cases. This result is complicated by the nontrivial response of each limit to background rates. Indeed, if one compares the first-generation solar and reactor limits in Fig. 3, the solar scattering disadvantage is more pronounced than predicted. However, the lower-background second-generation limit ratios are broadly consistent with the simplified expectation. Similarly, as the recoil sensitivity threshold is reduced sufficiently to access the ^{7}Be and pep line sources in Fig. 5, one sees discrete improvements in sensitivity consistent with predictions around 5–6 (scalar, axial vector) or 2–3 (vector) corresponding to escalation of the flux by a factor of around 30.

Finally, in the large mediator mass region, $2m_N E_r \ll m^2$, we can estimate the order of Q' by comparing the BSM "charge" to the SM charge: $\frac{1}{\sqrt{2}G_F} \frac{Q'_v}{m_z^2} = \frac{1}{2} Q_v$, so $Q' = \frac{\sqrt{2}}{2} m^2 G_F Q_v$. In order to distinguish BSM from SM signal, one should need Q' larger than this value.

[1] R. Essig *et al.*, Report No. YITP-SB-36.
[2] D. Z. Freedman, Phys. Rev. D **9**, 1389 (1974).
[3] L. M. Krauss, Phys. Lett. B **269**, 407 (1991).
[4] J. Barranco, O. G. Miranda, and T. I. Rashba, J. High Energy Phys. 12 (2005) 021.
[5] J. Barranco, O. G. Miranda, and T. I. Rashba, Phys. Rev. D **76**, 073008 (2007).
[6] A. N. Khan, Phys. Rev. D **93**, 093019 (2016).
[7] J. A. Formaggio, E. Figueroa-Feliciano, and A. J. Anderson, Phys. Rev. D **85**, 013009 (2012).
[8] P. deNiverville, M. Pospelov, and A. Ritz, Phys. Rev. D **92**, 095005 (2015).
[9] T. S. Kosmas, O. G. Miranda, D. K. Papoulias, M. Tortola, and J. W. F. Valle, Phys. Rev. D **92**, 013011 (2015).
[10] T. S. Kosmas, O. G. Miranda, D. K. Papoulias, M. Tortola, and J. W. F. Valle, Phys. Lett. B **750**, 459 (2015).
[11] B. Dutta, R. Mahapatra, L. E. Strigari, and J. W. Walker, Phys. Rev. D **93**, 013015 (2016).
[12] B. Dutta, Y. Gao, R. Mahapatra, N. Mirabolfathi, L. E. Strigari, and J. W. Walker, Phys. Rev. D **94**, 093002 (2016).
[13] M. Lindner, W. Rodejohann, and X.-J. Xu, J. High Energy Phys. 03 (2017) 097.
[14] J. R. Wilson, Phys. Rev. Lett. **32**, 849 (1974).

[15] M. Prakash, J. M. Lattimer, J. A. Pons, A. W. Steiner, and S. Reddy, Lect. Notes Phys. **578**, 364 (2001).

[16] C. J. Horowitz, K. J. Coakley, and D. N. McKinsey, Phys. Rev. D **68**, 023005 (2003).

[17] A. Burrows, S. Reddy, and T. A. Thompson, Nucl. Phys. **A777**, 356 (2006).

[18] H.-T. Janka, K. Langanke, A. Marek, G. Martinez-Pinedo, and B. Mueller, Phys. Rep. **442**, 38 (2007).

[19] A. N. Khan, D. W. McKay, and F. Tahir, Phys. Rev. D **88**, 113006 (2013).

[20] P. Coloma, J. High Energy Phys. 03 (2016) 016.

[21] S. K. Agarwalla, P. Bagchi, D. V. Forero, and M. Tortola, J. High Energy Phys. 07 (2015) 060.

[22] A. Drukier and L. Stodolsky, Phys. Rev. D **30**, 2295 (1984).

[23] B. Cabrera, L. M. Krauss, and F. Wilczek, Phys. Rev. Lett. **55**, 25 (1985).

[24] D. Akimov *et al.*, Science **357**, 1123 (2017).

[25] A. Aguilar-Arevalo *et al.* (CONNIE Collaboration), J. Phys. Conf. Ser. **761**, 012057 (2016).

[26] H. Bin Li (TEXONO Collaboration), J. Phys. Conf. Ser. **718**, 062036 (2016).

[27] G. Agnolet *et al.* (MINER Collaboration), Nucl. Instrum. Methods Phys. Res., Sect. A **853**, 53 (2017).

[28] J. Billard, L. Strigari, and E. Figueroa-Feliciano, Phys. Rev. D **89**, 023524 (2014).

[29] F. Ruppin, J. Billard, E. Figueroa-Feliciano, and L. Strigari, Phys. Rev. D **90**, 083510 (2014).

[30] J. B. Dent, B. Dutta, J. L. Newstead, and L. E. Strigari, Phys. Rev. D **93**, 075018 (2016).

[31] J. B. Dent, B. Dutta, J. L. Newstead, and L. E. Strigari, Phys. Rev. D **95**, 051701 (2017).

[32] R. Harnik, J. Kopp, and P. A. N. Machado, J. Cosmol. Astropart. Phys. 07 (2012) 026.

[33] D. G. Cerdeño, M. Fairbairn, T. Jubb, P. A. N. Machado, A. C. Vincent, and C. Bœhm, J. High Energy Phys. 05 (2016) 118.

[34] S. G. Porsev, K. Beloy, and A. Derevianko, Phys. Rev. Lett. **102**, 181601 (2009).

[35] B. C. Canas, E. A. Garces, O. G. Miranda, M. Tortola, and J. W. F. Valle, Phys. Lett. B **761**, 450 (2016).

[36] J. Erler and M. J. Ramsey-Musolf, Phys. Rev. D **72**, 073003 (2005).

[37] M. Cirelli, E. Del Nobile, and P. Panci, J. Cosmol. Astropart. Phys. 10 (2013) 019.

[38] P. Agrawal, Z. Chacko, C. Kilic, and R. K. Mishra, arXiv:1003.1912.

[39] K. R. Dienes, J. Kumar, B. Thomas, and D. Yaylali, Phys. Rev. D **90**, 015012 (2014).

[40] R. J. Hill and M. P. Solon, Phys. Rev. D **91**, 043505 (2015).

[41] C. Alexandrou, M. Constantinou, K. Hadjiyiannakou, K. Jansen, C. Kallidonis, G. Koutsou, A. V. Aviles-Casco, and C. Wiese, Phys. Rev. Lett. **119**, 142002 (2017).

[42] P. Klos, J. Menéndez, D. Gazit, and A. Schwenk, Phys. Rev. D **88**, 083516 (2013); **89**, 029901(E) (2014).

[43] E. Aprile *et al.* (XENON100 Collaboration), Phys. Rev. Lett. **111**, 021301 (2013).

[44] W. C. Haxton, R. G. Hamish Robertson, and A. M. Serenelli, Annu. Rev. Astron. Astrophys. **51**, 21 (2013).

[45] F. P. An *et al.* (Daya Bay Collaboration), Chin. Phys. C **41**, 013002 (2017).

[46] V. I. Kopeikin, Yad. Fiz. **75N2**, 165 (2012) [Phys. At. Nucl. **75**, 143 (2012)].

[47] K. Schreckenbach, G. Colvin, W. Gelletly, and F. Von Feilitzsch, Phys. Lett. **160B**, 325 (1985).

[48] N. Mirabolfathi, H. R. Harris, R. Mahapatra, K. Sundqvist, A. Jastram, B. Serfass, D. Faiez, and B. Sadoulet, Nucl. Instrum. Methods Phys. Res., Sect. A **855**, 88 (2017).

[49] R. Agnese *et al.* (SuperCDMS Collaboration), Phys. Rev. Lett. **116**, 071301 (2016).

[50] V. Singh and H. T. Wong (TEXONO Collaboration), *Proc. Sci.*, AHEP2003 (2003) 053.

[51] H. T. Wong, H.-B. Li, J. Li, Q. Yue, and Z.-Y. Zhou, J. Phys. Conf. Ser. **39**, 266 (2006).

[52] D. Akimov *et al.* (COHERENT Collaboration), arXiv:1509.08702.

[53] G. Cowan, K. Cranmer, E. Gross, and O. Vitells, Eur. Phys. J. C **71**, 1554 (2011); **73**, 2501(E) (2013).

[54] J. B. Dent, L. M. Krauss, J. L. Newstead, and S. Sabharwal, Phys. Rev. D **92**, 063515 (2015).

[55] M. Pospelov, Phys. Rev. D **84**, 085008 (2011).